Iron quantification at the sub femtogram level in magnetite hybrid silica methacrylate core–shell nanocomposite particles by sp-ICP-MS

Antonia Toska, Dominique Foix, Antoine Bousquet, Nang-Htay Yin, Christophe Pécheyran, Joachim Allouche

COMMUNICATION

Iron quantification at sub femtogram level in magnetite hybrid silica methacrylate core-shell nanocomposite particles by sp-ICP-MS.

Received 00th January 20xx,
Accepted 00th January 20xx

DOI: 10.1039/x0xx00000x

Antonia Toska,[a] Dominique Foix, [a] Antoine Bousquet, [a] Nang-Htay Yin, [a] Christophe Pécheyran, [a] and Joachim Allouche *[a]

This study highlights the application of single particle (sp)-ICP-MS on the field of hybrid (inorganic/organic) nanocomposites characterization as a valuable tool for monitoring the inorganic metal nanoparticles (NPs) distribution over the total nanocomposite population as well as for synthesis conditions adaptation. Two types of magnetic nanocomposites carrying iron oxide NPs either on the surface or in the core were synthesized in the laboratory and characterized by TEM, XPS and Auger mapping for confirmation of iron localization. Analysis of ^{56}Fe by sp-ICP-MS provided key information about the mass of iron integrated into each nanocomposite,at the sub femtogram level, which was directly correlated to their nanostructuration.

Hybrid metal or metal oxide organic-inorganic nanocomposites have been widely studied over the past several decades because of their great potential in many applications, from catalysis to biomedical ones.[1–4] Some of the most important efforts in the past 20 years have been devoted to the design and development of multifunctional core–shell nanomaterials to provide several functions in one single platform.[5–8] In this context, the design of hybrid nanocomposite particles embedding iron oxide colloids has undergone intensive investigations due to their potential, notably in nanomedicine.[9,10] However, the main challenge in their elaboration lies in the precise control of several structural, morphological, chemical and/or physico-chemical parameters to fine-tune the final properties. Indeed, a subtle balance between a high iron oxide colloids loading and a good dispersion within the encapsulating materials has to be optimized to guarantee enhanced properties.[11–13] Furthermore, achieving the stability of the hybrid nanocomposites and ensuring a suitable surface chemistry are essential for enabling further functionalization steps.[14] Therefore, a precise post-synthesis quantification of iron oxide nanoparticles (NPs) entrapped in hybrid particles may be determinant to optimize and to provide a feedback of the elaboration conditions. Moreover, obtaining this quantification at the single particle level is crucial for establishing a comprehensive understanding of the collective magnetic behaviour for a given colloidal dispersion. However, this direct quantification is challenging since it requires highly sensitive analytical techniques able to accurately measure the amount of metal per single nanocomposite at the femtogram (fg) or picogram (pg) level for a large number of nanocomposites. Until now, such information is inaccessible using standard physico-chemical or microscopy techniques for the NPs characterization due to the difficulty of simultaneously obtaining metal quantification both at the single particle level and on a large set of composite particles. In this context, single particle Inductively Coupled Plasma Mass Spectrometry (sp-ICP-MS), is an emerging technique developed in the fields of environment, medicine or food industry as a direct and fast way of measuring NPs number concentration and their size distribution in liquid samples.[15–18] ICP-MS offers a number of advantages, including high sensitivity, excellent selectivity, a robust atomisation source for atomising solid NPs and rapid detection (≤ 100 µs). As the sp-ICP-MS approach is capable of quantifying chemical elements at the single particle level, it has been used successfully in the last years to characterize numbers of metal or metal oxide colloids including silver,[19] gold,[20] titanium oxide[21] and even iron oxides.[22] However, up to now, this technique has never been performed for monitoring the influence on iron oxide colloids distribution over core-shell hybrid nanocomposites after slight modifications on the synthesis conditions.

In this work, the application of sp-ICP-MS/MS on the characterization of magnetic nanocomposites for the iron (Fe) quantification per single nanocomposite obtained by different synthetic procedures is demonstrated for the first time. Two morphologies of synthetic magnetic nanocomposites with different loading and localization of iron colloids were obtained

[a] Université de Pau et des Pays de l'Adour, E2S UPPA, CNRS, Institut des Science Analytiques et Physico-chimie pour l'environnement et les matériaux (IPREM), 2 avenue du Président Angot, 64000 Pau.

by modulating the synthesis conditions. The influence of the structuration on the loading and the mass distribution of iron (Fe) per nanocomposite is herein discussed.

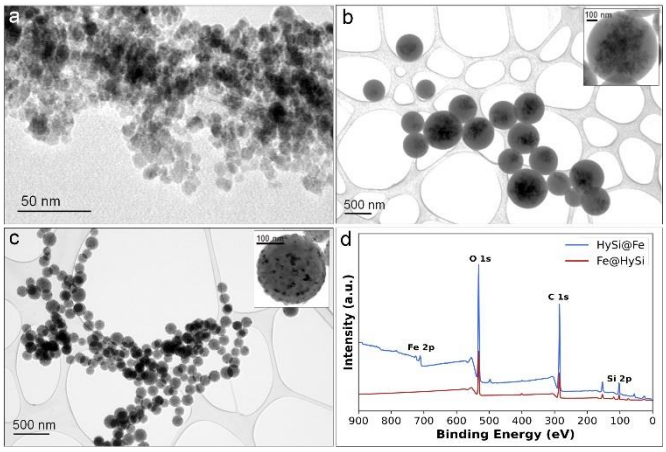

Figure 1. TEM images of (a) as synthesized iron oxide nanoparticles, (b) Fe@HySi, (c) HySi@Fe and (d) XPS survey spectra of Fe@HySi and HySi@Fe nanocomposites.

Magnetite iron oxide (Fe_3O_4) NPs were first synthesized by a classical Massart method.[23] TEM observation (Fig. 1a) of Fe_3O_4 NPs shows diameters of particles close to 8 ± 3 nm. X-ray photoelectron spectroscopy (XPS) analyses have been performed to identify the chemical environment and localization of Fe (experimental section ESI‡). Two different morphologies of synthetic magnetic nanocomposites, were then obtained depending on the elaboration conditions (ESI‡), for which the iron colloids have been either encapsulated in the core or adsorbed on the surface of the nanocomposites, namely Fe@HySi and HySi@Fe, respectively, where "HySi" stands for "hybrid silica polymer" and "Fe" for Fe_3O_4 NPs, the two materials composing both nanocomposites. For HySi@Fe, the structuration is governed by the initial formation of Pickering emulsion of (trimethoxysilyl)propyl methacrylate (TPM) droplets stabilized by Fe_3O_4 NPs. The final total nanocomposite diameter size can be tuned depending on the TPM/Fe_3O_4 weight ratio.[24,25] Like this, three different diameter sizes of HySi@Fe nanocomposites were obtained by modifying the TPM/Fe_3O_4 weight ratio from 0.03 to 0.16. The elaboration of Fe@HySi is lacking diameter size control and therefore only one TPM/Fe_3O_4 weight ratio of 0.16 was prepared for comparing the differences of Fe_3O_4 NPs distribution as a result of the different nanocomposites formation protocol.

The Fe@HySi and HySi@Fe nanocomposites prepared at the same TPM/Fe_3O_4 = 0.16 are displayed on the TEM images in Figures 1b and 1c, respectively. A difference of size and morphology between the two materials can be noticed. The median diameters calculated for the two materials are 480 nm and 146 nm for Fe@HySi and HySi@Fe respectively (see Fig. S1 and Table S1 ESI‡ for the complete nanocomposite size data obtained from the TEM images). For Fe@HySi (Fig. 1b), the images clearly exhibit iron colloids entrapped in the nanocomposite core highlighted by the high magnification picture (inset). In contrast, for HySi@Fe (Fig. 1c), the iron colloids are deposited on the surface of the nanocomposite sphere. XPS analyses of the nanocomposites provide additional information confirming the localization of the iron colloids for the two materials. Indeed, the XPS survey spectra in Fig. 1d show that Fe is only detected for HySi@Fe and is missing for Fe@HySi. Keeping in mind that the analysis depth of XPS is around 5-10 nm, this result is consistent with the surface deposition of iron colloids on the HySi@Fe composite spheres, the Fe being located in the core for Fe@HySi. (see the detail XPS characterization in ESI‡). To confirm the encapsulation of Fe_3O_4 NPs for Fe@HySi, Scanning Auger Mapping (SAM) analyses were also performed on cross-cut nanocomposites (Fig. S4 ESI‡). The elemental maps of Fe, Si and O from the analysis on one single composite particle allows to confirm the in-depth location of Fe in the hybrid composite sphere since Fe is only detected within the core.According to these results, the localization of Fe_3O_4 NPs depends on the structuration process of the nanocomposites elaborated. Such structuration is strongly influenced by the synthesis conditions which is considered to also affect the amount and the distribution of the Fe_3O_4 NPs in the whole set of the composite particles.

Consequently, to monitor the Fe_3O_4 NPs distribution per single nanocomposite, sp-ICP-MS/MS analyses have been performed by monitoring ^{56}Fe. An Agilent 8900 ICP-MS/MS instrument (semiconductor version) was used in tandem MS mode and H_2 as a reaction gas to unravel ArO interferences on ^{56}Fe. The natural abundance ratio of ^{56}Fe to ^{57}Fe (43.3) was systematically controlled before each analysis to confirm the effective ArO interferences elimination through the chosen instrumental conditions. For ensuring the measurement of single nanocomposites per reading time, while minimizing the probability of counting two particles at the same time, highly diluted nanocomposites samples were analysed with the fastest acquisition time of 0.1 ms and signal intensities were recorded as a function of time in a Time Resolved Analysis (TRA). The dilution level of each sample in Milli-Q water was adjusted so that the detected particle events per minute to be in the range of 600-1200. Sonication for few minutes was performed between each dilution and before the start of the analysis. Size certified gold NPs (BioPure Gold Nanospheres – bare, citrate stabilized, 50 nm, Nanocomposix, Clinisciences, France) were used for the calculation of the nebulization efficiency (η_n) through the detection of ^{197}Au under the same sample introduction conditions, based on the size reference material approach described by Pace *et al.*[26] Then the Fe mass distribution was calculated from the response factor calibration measured by analyzing Fe ionic solution at 1 ppb in nitric acid (HNO_3) 1 %. The operating conditions of ICP-MS/MS are provided in Table 1. For each sample, three replicate dilutions were prepared and used for the calculation of an average median Fe mass embedded per single nanocomposite. The combined uncertainties of the iron average median mass values for each mass distribution were calculated from the measurements of the replicates. To assess the possible agglomeration over time, the 3 replicate measurements were not performed successively to each other, but repeating the sample list with the same order.

Due to the very small diameter of the Fe_3O_4 nanoparticles (around 8 nm, see TEM observation Fig. 1a), it was not possible to measure their mass distribution using the sp-ICP-MS approach under the specific operating conditions.Indeed, the presence of an ionic Fe background in the solution hindered the discrimination of very small single particles against the background. In addition, note that a single 8 nm Fe_3O_4 NPs contains only about 0.98 attograms of iron, making its detection difficult even with the high sensitivity of ICP-MS/MS instruments.

The Figure 2 highlights the Fe mass distribution per nanocomposite obtained for Fe@HySi (Fig. 2a, TPM/Fe_3O_4 = 0.16) and HySi@Fe at TPM/Fe_3O_4 = 0.16 (Fig. 2b), 0.07 (Fig. 2c) and 0.03 (Fig. 2d), as well as the respective average median masses of the three replicate dilutions. At the same time, for 1 of the 3 replicate mass distributions, complete statistical analysis was performed using the ^{56}Fe peak integrated signal intensities recorded during 1 minute of acquisition time. All intensities above the particle threshold (calculated by the MassHunter software and presented in Table S3 ESI‡) were used for the statistical calculation of the median, mean and standard deviation of the Fe mass distribution. Finally, the Fe mass polydispersity index (PDI) was calculated as the square of the standard mass deviation divided by the square of the mean mass of the distribution. The PDI values calculated for each mass distribution are also displayed in Figure 2, while all statistical results are summed up on Table S3 (ESI‡). It is worth mentioning that the Fe particle threshold in the case of Fe@HySi nanocomposites is much higher compared to that of HySi@Fe. The latter observation was attributed to incomplete Fe_3O_4 NPs encapsulation in the core of the Fe@HySi nanocomposites, resulting in free Fe_3O_4 NPs whose signal is recorded as ionic Fe background, due to their small size. On the other hand, thanks to the formation of the Pickering emulsion all Fe_3O_4 NPs are stabilised on the surface of TPM droplets, while TPM excess is expelled by the system. As a result, in this case the particle threshold is only affected by the ionic Fe naturally present in Milli-Q or/and dissolved from the NPs during sonication. Due to the high Fe mass polydispersity in some samples, the mass distributions are not represented on the full abscissa axis. However, the box plots data are added to provide all the Fe masses detected and to better illustrate the

Table 1: ICP-MS/MS operation conditions

RF Power	1500
RF Matching (V)	1.3
Sample Depth (mm)	7.0
Nebulizer Gas (L/min)	0.7
Cell focus (V)	-2.0
Cell Entrance (V)	-50
H_2 flow (ml/min) in the collision/reaction cell	5.0
Isotope monitored during the Sp-ICPMS analysis and quadrupoles settings	^{56}Fe Q1 @ m/z= 56, Q2@ m/z=56
Dwell time (msec)	0,1
Nebulizer	Micromist DC 0.4 mL/ min
Spray chamber	Scott double pass cooled at 2°C
^{56}Fe / ^{57}Fe (1ppb solution as Fe)	43.2 (theoretical value : 43.3)

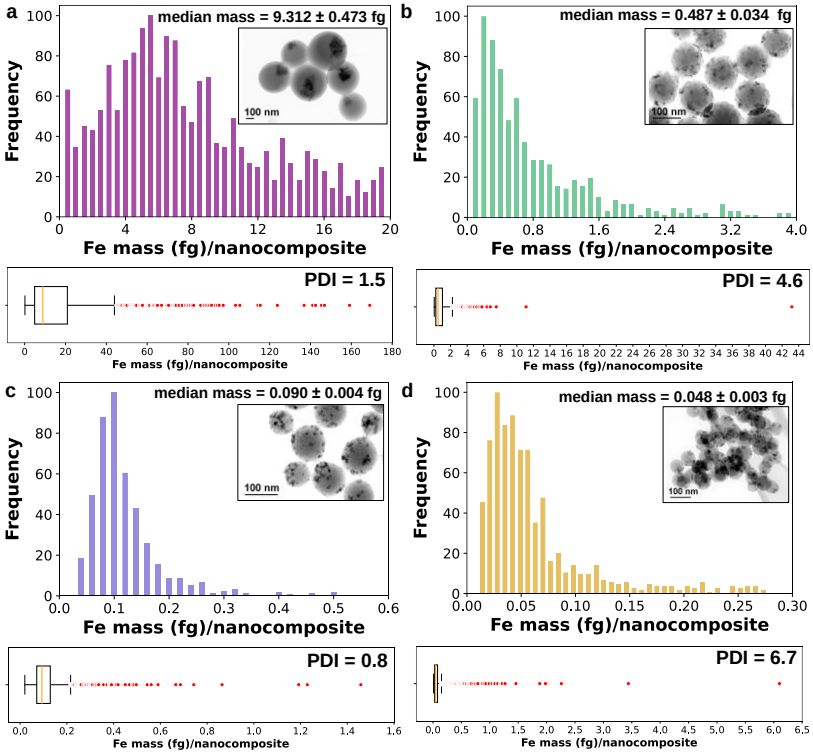

Figure 2. Iron mass distributions measured by sp-ICP-MS/MS, box plot data with the corresponding median masses and mass polydispersity index (PDI) for (a) Fe@HySi at TPM/Fe_3O_4 = 0.16, (b) HySi@Fe at TPM/Fe_3O_4 = 0.16, (c) HySi@Fe at TPM/Fe_3O_4 = 0.07 and (d) HySi@Fe at TPM/Fe_3O_4 = 0.03.

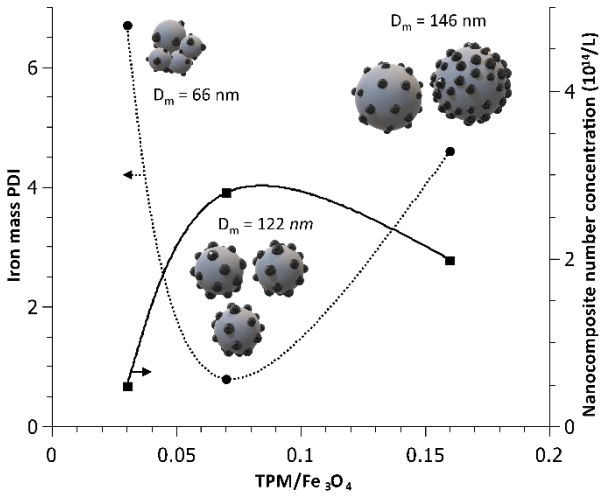

Figure 3. Evolution of the nanocomposite number concentration and nanocomposite median diameter as a function of the TPM/Fe_3O_4 ratio. (D_m : nanocomposite median diameter measured by TEM)

mass polydispersity for each sample. For TPM/Fe_3O_4 = 0.16, it is worth noting that the Fe amount entrapped in the composites is close to 20 times higher for Fe@HySi than for HySi@Fe with median masses of 9.31 ± 0.47 fg and 0.49 ± 0.03 fg respectively. The PDI value for Fe@HySi is 1.5 which is significantly lower than that of HySi@Fe (PDI = 4.6) indicating an increase in the heterogeneity of the Fe_3O_4 NPs distribution over the composite particles for HySi@Fe. Since the TPM/Fe_3O_4 is identical for those materials, the amount of iron oxide colloids per nanocomposite and their distribution over the composites are governed by the mechanisms of structuration of the materials. Indeed, for HySi@Fe, the structuration is directed by a thermodynamic process for which a Pickering emulsion is initially spontaneously formed.[25] The TPM/water interface generated by the small droplets is stabilized by the iron oxide colloids before silica condensation and acrylate polymerization. Due to the low surface area of each droplet, this leads to the deposition of sub femtogram amount of Fe on each nanocomposite. On the contrary, the structuration of Fe@HySi is mainly guided by a sol-gel process leading to the growth of a hybrid silica shell around Fe_3O_4 NPs aggregates core. Higher amount of iron oxide colloids encapsulated within the core of composite particles are detected in this case. However, the number of nanocomposites formed is 4 times less important in the case of Fe@HySi (Table S3, ESI‡).

The influence of the TPM/Fe_3O_4 ratio on the Fe_3O_4 NPs distribution in HySi@Fe was then investigated. The TPM/Fe_3O_4 ratio was modified by changing the amount of TPM while keeping the mass of Fe_3O_4 NPs constant. Consequently, the nanocomposite sizes are correlated to the evolution of the TPM amount since the number of iron colloids available for the stabilization of the interface generated by the Pickering emulsion is constant. The sp-ICP-MS/MS analyses performed on these samples provide Fe mass distributions showing a decrease of the global amount of Fe per nanocomposite with median masses of 0.49 ± 0.03 fg, 0.090 ± 0.004 fg and 0.048 ± 0.003 fg for TPM/Fe_3O_4 = 0.16, 0.07 and 0.03, respectively (Fig. 2b to 2d). This evolution is correlated to the reduction of the surface area of the Pickering droplets stabilized by the magnetic colloids. Indeed, as shown on the Fig. S1 and Table S1 (ESI‡), the median diameter of the nanocomposites decreases from 146 nm to 66 nm when the TPM/Fe_3O_4 drops. Concomitantly, the Fe mass PDI curve plotted as a function of the TPM/Fe_3O_4 ratio in Figure 3 reaches a minimum at 0.8 for TPM/Fe_3O_4 = 0.07 (Fig. 2c). The nanocomposite number concentration was also extracted from the sp-ICP-MS/MS data and represented on the same figure (Fig. 3) as a function of the TPM/Fe_3O_4 ratio (see Table S3 ESI‡, for the resume of the sp-ICP-MS/MS data). At TPM/Fe_3O_4 = 0.03, a low amount of nanocomposites number was detected by sp-ICP-MS/MS. This was attributed to the particle aggregation, as confirmed in the Figure 2d TEM picture inset, leading to double particle events during the sp-ICP-MS analysis. When the TPM volume increases, the nanocomposite number concentration detected follows an opposite trend of the PDI with a maximum of $2.77.10^{14}$ particles/L obtained for TPM/Fe_3O_4 = 0.07. At this TPM/Fe_3O_4 value, a best compromise is obtained between the Fe_3O_4 NPs concentration and the TPM volume leading to a good stabilization of the TPM/water interface and a good homogenous Fe_3O_4 NPs distribution over the nanocomposites during the Pickering emulsion formation.

Finally, this work demonstrates the great potential of sp-ICP-MS on the synthesis of inorganic/organic nanocomposites field, as a powerful tool able not only to elucidate the distribution of metal NPs over hybrid nanocomposites, but also to provide information valuable for the tuning of the synthesis conditions. In the specific case, Fe quantification per magnetic nanocomposite at femtogram level has been used to correlate the Fe mass distributions to the nanocomposite morphologies. In the case of the particles generated by Pickering emulsion, an accurate TPM/Fe_3O_4 ratio has been identified offering the best conditions and compromise in terms of nanocomposite size, stability and Fe_3O_4 NPs distribution. The characterization of the nanocomposite magnetic features is currently in progress to establish the full picture of the relationship between the Fe_3O_4 NPs distribution and the final material properties. Such sp-ICP-MS approach may be applied to a wide range of multifunctional hybrid colloid material for which the post-synthesis quantification of functional entities at the single particle level is crucial for the complete characterization of the final material.

Conflicts of interest

There are no conflicts to declare.

Notes and references

1 B. M. Novak, *Adv. Mater. Weinh. Ger.*, 1993, **5**, 422–33.
2 J. Kao, K. Thorkelsson, P. Bai, B. J. Rancatore and T. Xu, *Chem. Soc. Rev.*, 2013, **42**, 2654–2678.
3 E. Omanović-Mikličanin, A. Badnjević, A. Kazlagić and M. Hajlovac, *Health Technol.*, 2020, **10**, 51–59.

4 M. Yusefi, K. Shameli, H. Jahangirian, S.-Y. Teow, L. Afsah-Hejri, S. N. A. Mohamad Sukri and K. Kuča, *Int. J. Nanomedicine*, 2023, **18**, 3535–3575.
5 S. Wei, Q. Wang, J. Zhu, L. Sun, H. Lin and Zhanhu. Guo, *Nanoscale*, 2011, **3**, 4474–4502.
6 R. Ghosh Chaudhuri and Santanu. Paria, *Chem. Rev. Wash. DC U. S.*, 2012, **112**, 2373–2433.
7 K. Chatterjee, S. Sarkar, K. Jagajjanani Rao and Santanu. Paria, *Adv. Colloid Interface Sci.*, 2014, **209**, 8–39.
8 N. Habibi, D. F. Quevedo, J. V. Gregory and J. Lahann, *WIREs Nanomedicine Nanobiotechnology*, 2020, **12**, e1625.
9 R. van der Meel, E. Sulheim, Y. Shi, F. Kiessling, W. J. M. Mulder and T. Lammers, *Nat. Nanotechnol.*, 2019, **14**, 1007–1017.
10 M. Hepel, *Magnetochemistry*, 2020, **6**, 3.
11 M. Boissiere, J. Allouche, C. Chaneac, R. Brayner, J.-M. Devoisselle, J. Livage and Thibaud. Coradin, *Int. J. Pharm.*, 2007, **344**, 128–134.
12 M. Boissiere, J. Allouche, R. Brayner, C. Chaneac, J. Livage and Thibaud. Coradin, *J. Nanosci. Nanotechnol.*, 2007, **7**, 4649–4654.
13 J. Allouche, C. Chanéac, R. Brayner, M. Boissière and T. Coradin, *Nanomaterials*, 2014, **4**, 612–627.
14 S. Liu, B. Yu, S. Wang, Y. Shen and H. Cong, *Adv. Colloid Interface Sci.*, 2020, **281**, 102165.
15 E. Bolea, M. S. Jimenez, J. Perez-Arantegui, J. C. Vidal, M. Bakir, K. Ben-Jeddou, A. C. Gimenez-Ingalaturre, D. Ojeda, C. Trujillo and F. Laborda, *Anal. Methods*, 2021, **13**, 2742–2795.
16 K. Flores, R. S. Turley, C. Valdes, Y. Ye, J. Cantu, J. A. Hernandez-Viezcas, J. G. Parsons and J. L. Gardea-Torresdey, *Appl. Spectrosc. Rev.*, 2021, **56**, 1–26.
17 M. D. Montaño, J. W. Olesik, A. G. Barber, K. Challis and J. F. Ranville, *Anal. Bioanal. Chem.*, 2016, **408**, 5053–5074.
18 B. Meermann and V. Nischwitz, *J. Anal. At. Spectrom.*, 2018, **33**, 1432–1468.
19 N. J. Clark, R. Clough, D. Boyle and R. D. Handy, *Environ. Sci. Nano*, 2019, **6**, 3388–3400.
20 J. Jiménez-Lamana, L. Marigliano, J. Allouche, B. Grassl, J. Szpunar and S. Reynaud, *Anal. Chem.*, 2020, **92**, 11664–11672.
21 A. R. Donovan, C. D. Adams, Y. Ma, C. Stephan, T. Eichholz and H. Shi, *Chemosphere*, 2016, **144**, 148–153.
22 J. Nelson, A. Saunders, L. Poirier, E. Rogel, C. Ovalles, T. Rea and F. Lopez-Linares, *J. Nanoparticle Res.*, 2020, **22**, 304.
23 R. Massart, *IEEE Trans. Magn.*, 1981, **17**, 1247–1248.
24 S. Sacanna, W. K. Kegel and A. P. Philipse, *Langmuir*, 2007, **23**, 10486–10492.
25 S. Sacanna, W. K. Kegel and A. P. Philipse, *Phys. Rev. Lett.*, 2007, **98**, 158301.
26 H. E. Pace, N. J. Rogers, C. Jarolimek, V. A. Coleman, C. P. Higgins and J. F. Ranville, *Anal. Chem.*, 2011, **83**, 9361–9369.